JOURNAL OF COLLOID AND INTERFACE SCIENCE **185,** 94–103 (1997)
ARTICLE NO. CS964586

SPR Studies of the Nonspecific Adsorption Kinetics of Human IgG and BSA on Gold Surfaces Modified by Self-Assembled Monolayers (SAMs)

VITALII SILIN,*[,1] HOWARD WEETALL,† AND DAVID J. VANDERAH†

*Biotechnology Division, National Institute of Standards and Technology, Gaithersburg, Maryland 20899 and Department of Biology, Georgetown University, Washington, DC 20057-1028; and †Biotechnology Division, National Institute of Standards and Technology, Gaithersburg, Maryland 20899

Received April 23, 1996; accepted September 3, 1996

The nonspecific binding of human immunoglobulin G (hIgG) and bovine serum albumin (BSA) was studied on gold surfaces modified by self-assembled alkyl thiol monolayers (SAMs) with the following terminal groups: CH_3, C_6H_4OH, COO^-, NH_2, OH, and oligoethylene oxide (OEO). The kinetics of hIgG and BSA adsorption and desorption were monitored in real time utilizing the surface plasmon resonance (SPR) technique with a flow cell. The surface concentration of hIgG molecules adsorbed on the SAMs decreased in the order: $CH_3 > C_6H_5OH > COO^- > NH_2 > OH >$ OEO SAM surfaces. Binding of BSA to the SAM surfaces decreased in the order: $C_6H_5OH > CH_3 > COO^- > NH_2 > OH >$ OEO. The results show that on the OEO SAM, the surface concentration of these proteins was less than 0.5 ng/cm^2 (the detection limit of our SPR device) and approximately 10^3 times less than that on the hydrophobic CH_3-terminated SAM surfaces. The kinetics of the binding curves for the adsorption of the proteins are described in terms of multiple states of adsorbed proteins that involve multipoint hydrophobic, electrostatic, and hydrogen bond interactions for the different surfaces and protein lateral interactions caused by the unfolding of adsorbed proteins.

Key Words: **protein adsorption; self-assembled monolayers; SAMs; SPR.**

INTRODUCTION

Understanding the processes involved in the interactions of biomolecules with surfaces to which biomolecules are adsorbed has significant scientific and practical value (1–3). Many of the techniques that are currently used for investigation of biomolecular interactions in model systems, such as antigen–antibody complexation (4), cells receptor recognition of polypeptides or proteins (5), and DNA hybridization are based on the specific interaction between biomolecules in the bulk solution and species attached to various types of surfaces. Practical problems such as improvement of sensitivity and specificity of immunoassays and decreasing the interaction of human fluid (blood, tear, saliva) proteins with the surfaces of materials for use in clinical implants (6), contact lenses (7), and dental alloys (8) are related to protein adsorption activity and surface properties.

Extremely sensitive methods available for studying a biomolecule's interaction with a surface include surface plasmon resonance technique (9, 10), ellipsometry (11–17), total internal reflection fluorescence spectroscopy (18), and techniques based on protein labeling. Enzyme-linked antibodies (19) and radioactive isotopes, for example, can detect picomolar concentrations of analytes in solution. The detection limits of these techniques are not usually determined by either the specific biochemical reactions involved or the measurement techniques employed (fluorescence, radioactive radiation, evanescent surface electromagnetic waves, or light polarization) to observe protein adsorption. In most cases, sensitivity is limited by the nonspecific adsorption of biomolecules, which in turn depends on the biophysical and chemical properties of the adsorbed surface. It is well known (1, 2) that proteins adsorbed on a surface, as a rule, partially loose their bioactivity due to conformational changes in secondary structure and/or nonoptimal orientation and distribution on the surface. The protocols for preparation of surfaces (3) and the conditions of mass transport (20, 21) significantly influence the protein adsorption response. Therefore, quantitative comparison of data obtained from different laboratories becomes difficult. The investigation of protein adsorption kinetics and the detailed structure of protein films offers many challenges and difficulties. To obtain reproducible experimental data, it is necessary to use appropriate techniques that are sensitive enough to detect submonomolecular layers. The characteristics of the sorbent surfaces used should be well defined (22), and mass transport conditions must be controlled during experiments.

Over the past decade, the technique of preparing self-

[1] To whom correspondence should be addressed at Biotechnology Division, NIST, 222/A353, Gaithersburg, MD 20899.

0021-9797/97 $25.00

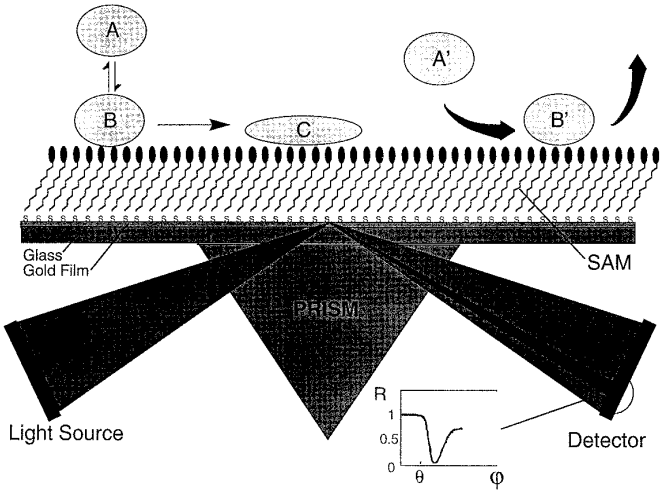

FIG. 1. Diagram of surface plasmon resonance technique applied to protein adsorption detected on a SAM-modified gold surface. *A*, *A′*, *B*, and *C* indicate proteins in the solution that can change conformation during irreversible or reversible adsorption. *R* is the reflection coefficient, φ is the angle of laser beam incidence, θ is the angle of total internal reflection.

assembled monolayers (SAMs) from solutions containing alkyl thiols and ω-functionalized alkyl thiols has been developed (23) for modifying noble metal (Au and Ag) surfaces. Gold surfaces modified using SAMs with various terminal groups provide surfaces with a wide range of different characteristics (23). Moreover, these surfaces are at least quasi-crystalline, stable, and reproducible. It has been shown (24, 25) that the SAM surface is a well-defined system for examining the interaction between proteins and surfaces and enables one to test ideas regarding the mechanisms of these interactions.

An excellent method for the *in situ* investigation of protein adsorption is surface plasmon resonance (SPR) (9, 10, 20). This method enables the direct monitoring, without labeling the analyte, of the kinetics of the interactions between proteins and a surface in real time. The observation of a SPR shift, during protein layer formation on a surface, gives information about the surface concentration of the proteins (10, 26).

The SPR excitation on metal films is observed (Fig. 1) as a dark band in the *p*-polarized light reflected from the bottom of a glass prism coated with a thin (~50 nm) metal film. The SPR phenomenon is dependent upon the coupling of light with surface modes associated with collective electron oscillations within the metal film. Plasmon resonance may be achieved by employing an evanescent wave resulting from a light beam being totally internally reflected inside a medium of higher dielectric constant that is interfaced with one of a lower dielectric constant. An example of this is a glass prism interfaced with a buffer. In the widely used Kretschmann configuration (9), a thin metal film is deposited on the base of a prism. The SPR resonance may be observed by monitoring the reflected light intensity versus the angle of the incidence of the light beam within the prism. It is known (9) that the SPR minimum position, as measured by the angle of the light incident on the metal surface, depends on the thicknesses and refractive indexes of all layer structure components on the metal surface and the optical properties of the medium that is in contact with the sample surface. This phenomenon is used for measurement of protein adsorption on the modified gold surface in real time. When the thickness of the protein layer increases during adsorption, SPR shifts and minima location correspond to the amount of protein on the surface.

The purpose of this report is to examine by SPR, in real time, the adsorption kinetics of the proteins BSA and hIgG to a well-defined gold surface modified by alkyl thiols (Table 1) with different terminal functional groups: CH_3, COO^-, OH, PheOH, NH_2, and OEO. BSA and hIgG were chosen because: (i) they are important to immunoassay design, (ii) their adsorption characteristics have been well studied on a variety of surfaces (1–3), and (iii) they have opposite net charges.

MATERIALS AND METHODS

Materials

BSA and human IgG were purchased from Sigma Chemical Company (St. Louis, Missouri).[2] Proteins were dissolved in 50 m*M* sodium phosphate buffer, pH 7.4, to a final concentration 0.5 μM. All protein solutions were prepared with high purity (18.2 $M\Omega$) water. Before use, the buffer was filtered through a 0.2 μm filter and degassed with argon. The CH_3 and NH_2 thiols were purchased from Aldrich Chemical Company (Milwaukee, Wisconsin). The COO^-, OH, and OEO thiols were prepared according to previously published literature procedures (27). The PheOH thiol has been not previously described in the literature. Details of the synthesis of this compound will be reported elsewhere. Purity of all thiols (>98%) was determined by proton nuclear magnetic resonance (^{1}H NMR) on a Bruker FM-400 spectrometer which indicated the presence of disulfide (<2%) as the only significant impurity.

Sample Preparation

The samples were polished glass substrates of size 20 mm × 14 mm × 2 mm. Before deposition of the gold film the glass substrates were cleaned by washing with (1) detergent, (2) Nochromix-sulfuric acid solution (overnight), (3) dis-

[2] Certain commercial equipment, instruments, and materials are identified in this paper to specify adequately the experiment procedure. In no case, does such identification imply recommendation or endorsement by the National Institute of Standards and Technology nor does it imply that the material or equipment is necessarily the best available for the purpose.

TABLE 1
List of Alkyl Thiols Used for Self-Assembled Monolayers Formation on the Gold Surfaces

#	Name of Alkyl Thiol	Chemical Formula	Abbreviation
1	16-hexadecanethiol	$HS(CH_2)_{15}CH_3$	(CH_3)
2	16-mercaptohexadecanoic acid	$HS(CH_2)_{15}CO_2H$	(COO^-)
3	16-mercaptohexadecanol	$HS(CH_2)_{16}OH$	(OH)
4	*p*-(12-mercapto-1-oxododecanyl) phenol	$HS(CH_2)_{11}COC_6H_4OH$	(PheOH)
5	2-aminoethanethiol	$HS(CH_2)_2NH_2$	(NH_2)
6	Oligoethylene oxide (11-mercaptoudecyl hexa(ethylene oxide))	$HS(CH_2)_{11}(OCH_2CH_2)_6OH$	(OE)

tilled water until the pH of water was ~6, (4) concentrated sodium hydroxide solution (15–20 min), (5) distilled water until the pH of the water was ~6, (6) high purity (18.2 $M\Omega$) water, and (7) high purity (99.99) acetone and then dried in a nitrogen gas stream. The gold film was deposited on the polished glass substrate surface in a thermal metal evaporation device (Denton Vacuum model DV-502A) at vacuum of 10^{-7} torr. The rate of gold evaporation and the film thickness were controlled by a quartz resonance sensor. The conditions of gold film preparation, to give a gold film thickness of 490 Å, were evaporation rate 12 Å/s and annealing time 45 min. Immediately after removal from the vacuum chamber (not more than 3–5 min), each sample was introduced into a 1 m*M* solution of thiol in ethanol. Incubation time was overnight. Before making measurements, all samples were washed in 200 proof anhydrous ethyl alcohol for 30 min and then dried in a nitrogen gas stream. Each sample was prepared separately.

Contact angle measurements were carried out using a Rame-hart, Inc., NRL C.A. goniometer.

The SPR Apparatus

The SPR setup consisted of an optical measuring unit, a flow cell (volume 30 μL), a peristaltic pump, a manual injection system, and a computer with the appropriate software specially designed for this device. The optical measuring unit consisted of a semiconductor laser (750 nm), a polarizer to create *p*-polarized light on the bottom of the prism, a beam expander to increase beam size by approximately a factor of ten, a cylindrical lens to focus the laser beam on the sample with an angle distribution of ~10°, and a CCD detector with 512 pixels. The main elements of the setup were a glass prism and a flow cell (Fig. 2) with a sample that is in optical contact with the glass prism. These elements were mounted on a rotating optical table with an angle resolution of 0.001°. The prism allowed the possibility of changing the laser beam incidence angle while simultaneously keeping the reflection beam in the same position on the CCD detector. This means that if the prism rotated around the axis that passed through the sample center, only the point of nonreflectance (Fig. 1), caused by the SPR excitation, shifted across the reflected beam.

Software, which was designed for the SPR setup, controlled the collection of real-time experimental data, smoothing of the experimental curves, and fast least-squares fit by linearization of a fitting Gaussian function to find the SPR minima position (in pixels) and SPR line width. The time to measure one point was ~10 s. The measured detection limit of the SPR device was ±0.1 pixel of the CCD. To carry out experiments close to the detection limit, the samples, buffers, and protein solutions must be prepared as described here. Any inhomogeneity in the solutions, impurities, or gas bubbles will lead to increased noise. Moreover, during the initial stages of incubation of a sample surface in the buffer or even in water, a SPR minimum shift is observed. The reasons for the effect are not clear. It is possible that this may be the result of swelling of the layer or exchange of alcohol with water molecules inside the SAM layer leading to changes in the optical properties of the SAM layer. Secondary Ion Mass Spectroscopy (SIMS) showed a large $C_2H_5O^-$ line with freshly prepared CH_3 SAM surfaces (unpublished results). The baseline usually stabilized after a 40–60 min exposure to the flowing buffer. After the baseline had stabilized, protein solution (0.5 μM) was introduced to the cell at the constant flow rate of 2.4 μL/s.

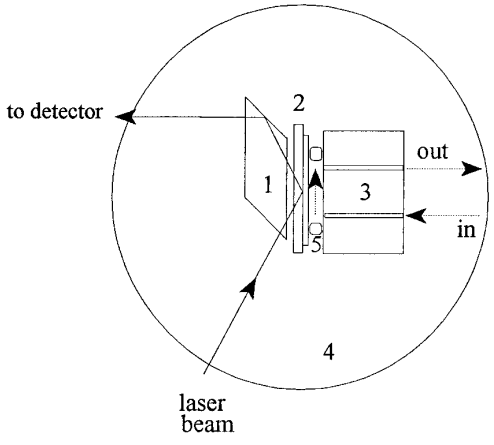

FIG. 2. Diagram showing the flow cuvette for SPR measurements: 1, glass prism; 2, sample; 3, Teflon base with input and output flow channels; 4, optical rotating table; 5, Teflon-encapsulated O rings. Measurement aperture was ~5 × 1 mm, cuvette volume ~36 μL, flow rate ~0.0024 ml/s, velocity of the fluid ~1.2 mm/s.

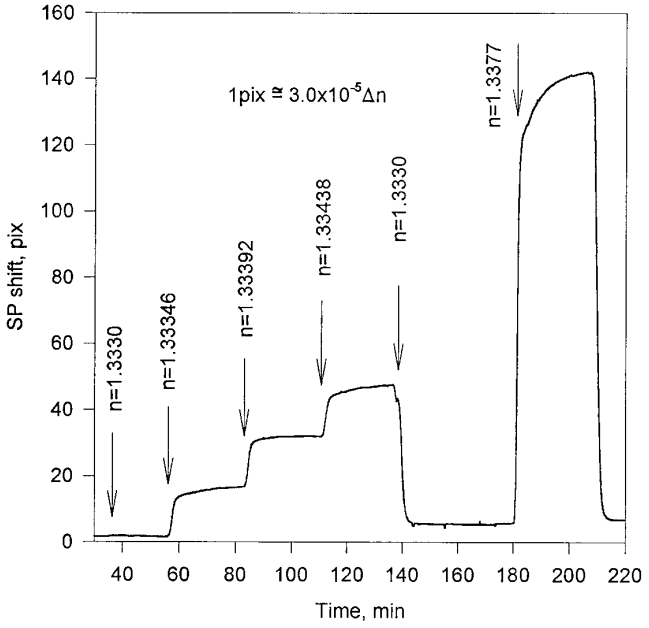

FIG. 3. The observed shift in the SPR minima versus the bulk refractive index of a water-glycerol solution. Arrows indicate the times when the solutions were changed. Concentrations of the glycerol in the water were 0, 4.06, 7.33, 12.18, and 40.6 mg/mL, respectively, to refractive indexes *n* of the solutions.

The calibration of the SPR device was carried out by two different methods. These two methods determined the relationship between the angle of the incidence of the light beam and the pixel number. The first was based on the glass prism geometry used for surface plasmon excitation. The angle was varied in the range of 1.5° using an optical rotation table. A linear correlation between the angle of the prism and pixel number was found (data not given). A simple calculation showed that one pixel corresponded to 0.0048°.

The second method was based on the dependence of the SPR minima location on the bulk refractive index of the media that is in contact with the sample surface. Figure 3 shows the SPR minima shift versus the well-known bulk refractive index of a water-glycerol solution. These measurements showed that one pixel corresponded to a change in the bulk refractive index of the solution of 3.0×10^{-5}. Using a theoretical model (26) for calculations and experimental data (Fig. 3), it was found that one pixel corresponded to 0.0053°. This value correlated well with data observed using the first method of the calibration. The difference was probably caused by the interaction of glycerol molecules with the surface. All curves in Fig. 3 show a fast and a slow portion of the SPR shift. The slow portion is probably due to the interaction of glycerol molecules with the surface leading to the formation of an intermediate layer on the gold surface.

The relation between thickness or surface concentration and pixel number was established by model calculations that correlated the multilayer structure characteristics and the position of the SPR angle. The theoretical model (26) used for calculations contained five media with parameters shown in Table 2. This model gave a linear dependence between the angle and layer thicknesses (it is only true for thicknesses less than ~400 Å) where 1 Å corresponded to 0.0083°, or one pixel of the SPR device corresponds to 0.60 Å.

Usually the values of the protein layer effective thicknesses d_p and effective refractive indexes n_p obtained by fitting a theoretical model with experimental data for films of less than 100 Å thickness have a considerable experimental scatter (12, 13). This scatter is covariant. Over- or underestimation of n_p corresponds, respectively, to under- or overestimations of d. The value of surface concentration M is calculated by the following formula, which is true for noninteracting particles (12)

$$M = d_p(n_p - n_b)/(dn/dc), \qquad [1]$$

where n_b is the refractive index of the buffer and dn/dc = 0.182 mL/mg (11). Using observed optical constants M can be determined with great accuracy in spite of fluctuating values of d_p and n_p (12) due to the covariance of these two parameters. The relationship between the surface concentration and pixel number was calculated using Eq. [1] and the parameters from Table 2. Thus, 1 pixel = 2.4 ng/cm^2, and the detection limit is less than 0.5 ng/cm^2.

Estimation of the calibration error for M was made by changing the refractive indexes and thicknesses in model calculations. The resulting calibration error was less than 7%. To improve on this will require additional investigations to estimate M using methods based on protein labeling or atomic force microscopy (AFM) studies.

RESULTS

Figures 4, 5, and 6 present our experimental results for hIgG and BSA adsorption on a series of SAM modified gold surfaces. Figure 4 shows the kinetics of adsorption of hIgG

TABLE 2

Parameters Used for Calculation of the Correlation between the SPR Minima Shift in Angle (degrees) During the Growth of the Biomolecular Layer (#4) Thickness (*d*)

#	Media	*n*	*k*	*d* (Å)
1	Glass prism	1.515	0.0	∞
2	Gold film on the prism base	0.174	4.86	490
3	SAM layer on gold film	1.45	0.0	21
4	Protein layer on SAM surface	1.40	0.0	0–400
5	Buffer solution	1.335	0.0	∞

Note. *n* and *k* are the real and imaginary parts of the refractive indexes.

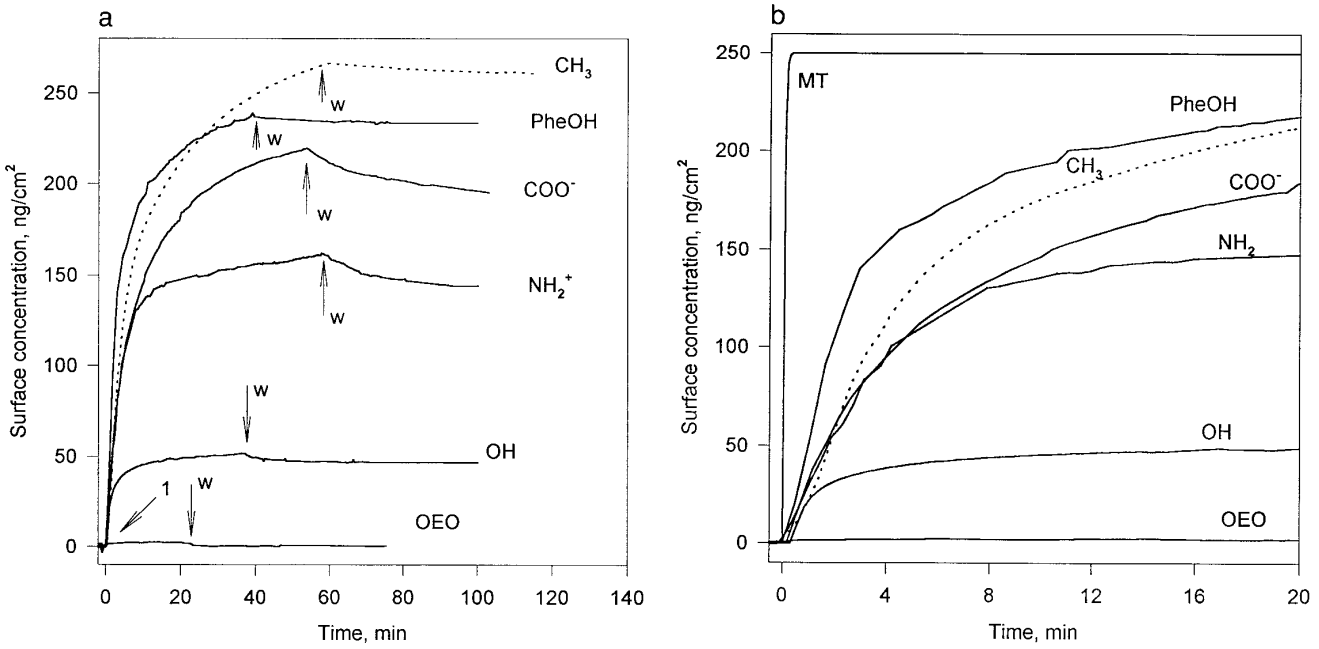

FIG. 4. (a) Kinetics of hIgG adsorption on gold surfaces modified with CH_3, PheOH, COO^-, NH_2, OH, and OEO SAMs. Arrow 1 shows time when the protein solution flow was started (hIgG concentration 0.5 μM), arrows marked *w* show time when washing was begun. (b) Initial stages of hIgG adsorption on the SAM surfaces. MT represents adsorption process with mass transport limitation.

(0.5 μM) on the different SAMs upon exposure to protein solutions and subsequent protein free buffer washes *w*. The surface concentrations (ng/cm^2) decreased in the order CH_3 (239) > PheOH (230) > COO^- (208) > NH_2 (161) > OH (58) > OEO (<0.5) with little desorption of protein (especially for CH_3 and PheOH) upon an extensive subsequent buffer wash. The highest hIgG surface concentration was obtained on the hydrophobic CH_3 SAM, and the lowest

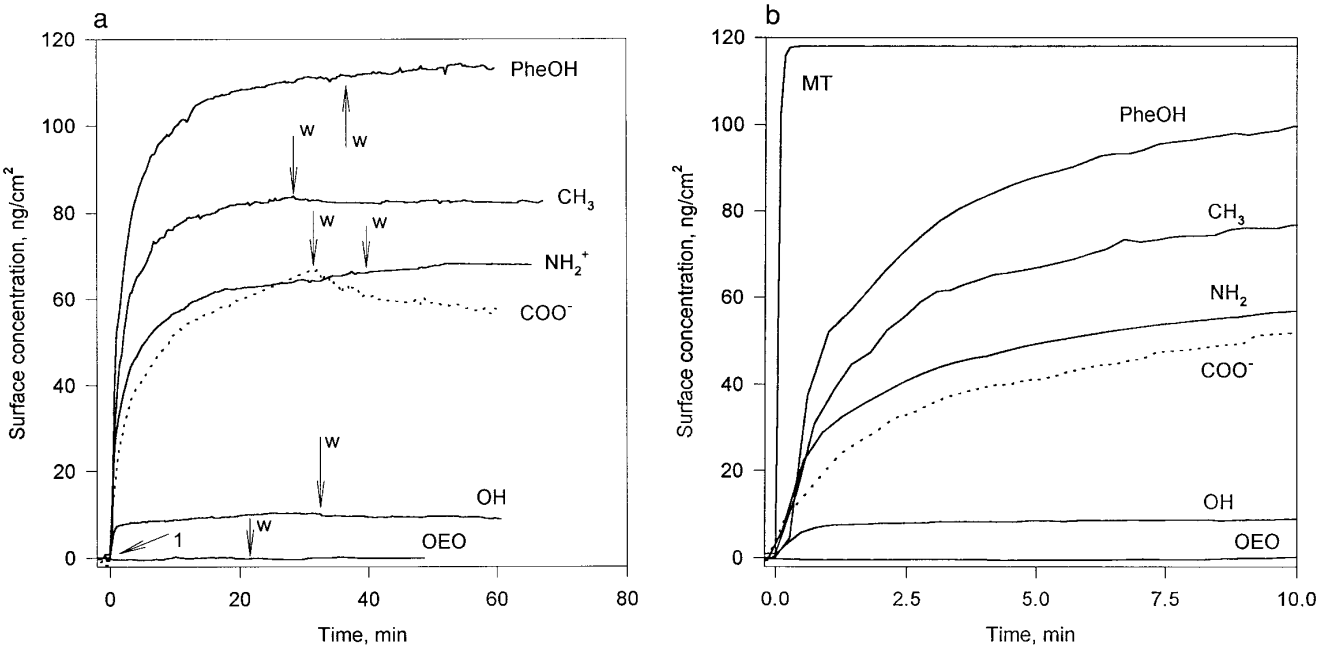

FIG. 5. (a) Kinetics of BSA adsorption on gold surfaces modified with CH_3, PheOH, COO^-, NH_2^+, OH, and OEO SAMs. Arrow 1 shows time moment when protein solution flow was started (BSA concentration 0.5 μM), arrows marked *w* show time when washing was begun. (b) Initial stages of BSA adsorption on the SAM surfaces. MT represents adsorption process with mass transport limitation.

was obtained on the moderately hydrophilic OEO SAM. The OEO data in Fig. 4 is different from the other SAMs, showing hIgG adsorption for three different protein concentrations of 0.5, 1.6, and 5.7 μM (points 1, 2, and 3, respectively) and subsequent buffer washes (points *w*). As can be seen, even a tenfold increase in protein concentration resulted only in a slight SPR shift that is reversed with subsequent buffer washing. The data in Fig. 4b also shows that the initial adsorption rates of hIgG vary for the different SAMs with the largest rate being observed for the PheOH SAM and the smallest for the COO^- SAM. In addition, at 0.5 μM hIgG, the rate of adsorption diminished with time but saturating levels of adsorption (i.e., $dM/dt = 0$) were not observed for all these SAMs even after one hour (data not shown).

Figures 5a and 5b show the adsorption kinetics of BSA on the different SAMs upon exposure to protein solution and subsequent protein free buffer washes. The surface concentrations (ng/cm^2) decreased in the order PheOH (111) > CH_3 (83) > COO^- (68) > NH_2 (63) > OH (10) > OEO (<0.5) with no significant desorption of BSA upon subsequent buffer wash. The highest BSA concentration was obtained on the PheOH SAM and the lowest was on the OEO SAM. Similar to Fig. 4, the OEO data in Fig. 5 are different from the other SAMs showing BSA adsorption for different protein concentration solutions (0.5 and 5.0 μM). The OEO data for BSA again show that a large increase in protein concentration resulted in only a slight SPR shift (no BSA adsorption observed for 0.5 and 1.65 μM concentrations), which is reversed with subsequent buffer washing. Initial adsorption rates for BSA were similar to those obtained for hIgG with the largest rate observed for the PheOH SAM. Like hIgG, saturating levels of adsorption ($dM/dt = 0$) were not observed for BSA on most of these SAMs. Moreover, for the PheOH SAM and the NH_2 SAM surface adsorption curves continued to increase after washing was begun.

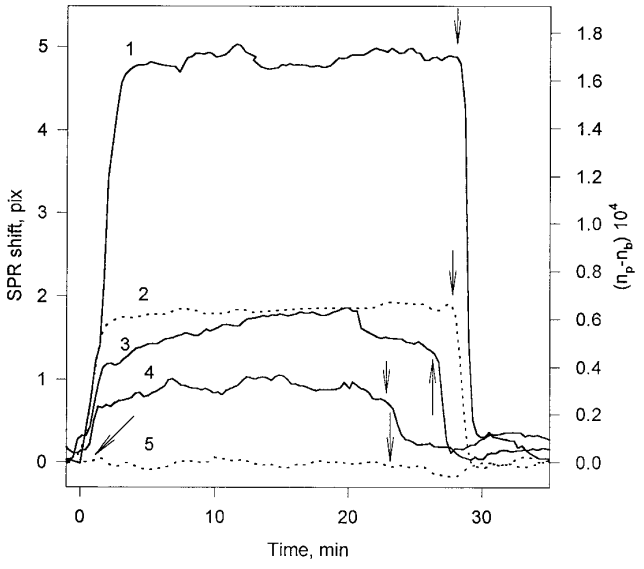

FIG. 6. Influence of the difference in bulk refractive index of protein solutions ($n_p - n_b$) to the SPR shift. n_p and n_b are bulk refractive indexes of the protein solutions and buffer, respectively. Solid lines correspond to the hIgG solutions, and dotted lines to BSA solution. Protein concentrations for curve 1 is 5.7 μM, 2 is 5.0 μM, 3 is 1.6 μM, and 4 and 5 are 0.5 μM. Arrows indicate time of introduction of the solution into the flow-cell and washing with buffer.

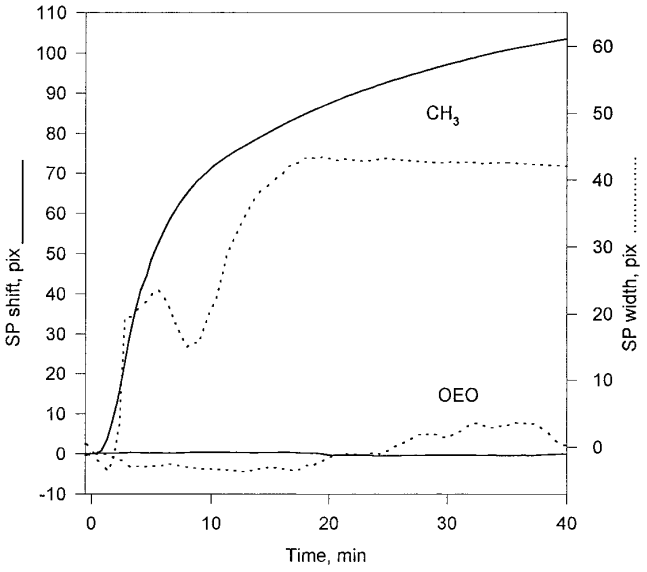

FIG. 7. Increasing of the SPR width (dotted lines) versus time of hIgG adsorption on CH_3 and OEO SAM surfaces. Solid lines are kinetics curves for these surfaces. Measurements of the SPR shift and SPR width were carried out simultaneously.

Comparison of the data for hIgG (Fig. 4) and BSA (Fig. 5) shows that, except for the OEO SAM, adsorption of hIgG was consistently higher than BSA. The ratio of the [hIgG]/[BSA] for the OH SAM was ~6/1; for the CH_3 SAM, COO^- and NH_2 SAM the ratio was ~3/1; and for the PheOH SAM the ratio was ~2/1. The adsorption concentration of hIgG was highest on the CH_3 SAM, whereas the adsorption concentration of BSA was highest on the PheOH SAM.

Figure 6 shows the adsorption kinetics of hIgG (solid lines) and BSA (dashed lines) onto different OEO SAM samples upon exposure to different protein concentrations and upon subsequent protein-free buffer washes.

The SPR width dependent on the molecular level surface inhomogeneity and, probably, can be a very good indicator of protein distribution and orientation on the surface. Figure 7 shows the SPR width changes versus time of hIgG adsorption on the CH_3 and OEO SAM surfaces. As can be seen, as the time of adsorption increased on the CH_3 SAM surface the SPR width increased significantly. For this surface a minimum in SPR width was observed after an adsorption time of approximately 8 min. In the case of OEO SAM surface the SPR width did not change. Our results for SPR width dependence on protein

adsorption for all studied surfaces will be presented elsewhere.

DISCUSSION

Our experimental kinetic curves show fast changes at initial stages of adsorption and significantly slower changes at later stages of adsorption. The influence of mass transport in our experiments was estimated by the methodology developed in (20)

$$m_l = 0.98D^{2/3}(u/hl)^{1/3}, \quad [2]$$

where m_l is the mass transfer coefficient, D is the diffusion coefficient of hIgG and BSA, u is a linear flow rate of the solution, l is the length for the biospecific active surface, and h is the channel height. Calculations, using experimental parameters presented in Fig. 2 caption and the methods section, and using $D = 3.26\ 10^{-7}$ cm^2/s for BSA and $2.3\ 10^{-7}$ cm^2/s for hIgG (20) resulted in values of $m_l = 1.59 \times 10^{-4}$ cm/s and 1.259×10^{-4} cm/s for BSA and hIgG, respectively. These values are on the order of one to two times larger than those usually obtained for rates of protein adsorption (12, 13). For comparison, in Figs. 4b and 5b curves (*MT*) show the hypothetical (one-exponent) protein adsorption process that corresponds to a rate constant equal to m_l. As can be seen, mass transfer, a limiting step in the kinetics of protein adsorption studies in nonflow experiments, is not a major factor under these experimental conditions.

The experimental results presented in Figs. 4–6 show that the nature of the SAM surface more strongly influences the amount of the adsorbed protein than the nature of these particular proteins (charge, amino acid sequence, shape, etc.). The difference between the surface concentrations of BSA and hIgG adsorbed on a given SAM surface is significantly less in terms of the number of the adsorbed molecule per cm^2, for these two proteins, than in terms of the mass (ng)/cm^2 because the molecular weight of the BSA is approximately half that of hIgG. As a rule, a higher molecular weight protein would more strongly interact with a surface due to increased multipoint attachments (1, 3) of the protein to the surface and, therefore, have higher binding energies of protein-surface interaction. This may result in an increase in protein surface concentration. Our attempts to apply first-order kinetics to calculate adsorption rates using a one-exponent model did not give a good fit to the experimental data. A two-exponent model, one that includes two reversible adsorption processes, gave a better fit, but the calculation does not provide a unique solution, since the results depend on the starting fitting parameters. The real model of protein adsorption is much more complex and involves many processes such as protein-interface interactions, protein orientations on the surface, conformational changes accompanied with protein unfolding, lateral protein-protein interactions, and desorption that lead to multiple states of adsorbed proteins on the surface (3). The presence of multiple states of adsorption probably is reflected in the changes in the SPR width versus adsorption time (Fig. 7). It is also necessary to point out (see Fig. 5 curves PheOH and NH_2, where one does not observe the decrease in protein adsorption after beginning of washing) that by the same reasoning, Eq. [1] cannot be used to prudently calculate surface concentration for all cases.

Consistent with earlier studies of hydrophobic surfaces (1–3, 15), we observed that the CH_3 SAM surface (contact angle = 105°) strongly adsorbed both BSA and hIgG. The strength of adsorption was indicated by a protein surface concentration (M) of approximately 85 and 260 ng/cm^2, respectively, and a resistance to desorption of protein during washing (see Figs. 4 and 5, CH_3 curves). This strong interaction is likely a complex process. Figure 7 shows an overall increase in SPR width with minimum during the first 8 min after exposure to protein solution. The broadening of the SPR line can be a result of the radiative damping of surface plasmon (26) due to increasing in inhomogeneity (molecular level roughness) of the sample surface during protein adsorption. In the case of the OEO surface, where little protein is adsorbed (Fig. 7, curve OEO), very little change in SPR width was observed. We suggest that, in the case of the CH_3 surface, the increase in SPR width and the observation of a minimum in the SPR width is indication of changes in protein distribution and conformation during adsorption. Probably, protein adsorption to this surface is a multistep process most likely initiated by hydrophobic residues on the protein surface. The initial interaction is then followed by multipoint interactions due to various degrees of the protein denaturation and/or cooperative effects (3). The low level of desorption of proteins from the CH_3 surface is consistent with strong adsorption forces and further supports the hypothesis of multipoint protein-surface interactions.

Surprisingly, the PheOH SAM surface also strongly adsorbed the studied proteins. The contact angle of this surface is 36°, and, therefore, the surface can be considered hydrophilic. Nonspecific adsorption of proteins to hydrophilic surfaces has been reported to be relatively low (1, 2). The terminal group of PheOH SAM can interact with BSA and hIgG in three ways: (i) hydrogen bonding with either the hydrogen or the oxygen atoms of the hydroxyl group, (ii) with the carbonyl group via either hydrogen bonding (oxygen atom only) or Schiff base formation, and (iii) $\pi - \pi$ interactions between π electrons in the protein and the π electrons of the phenol ring. At pH 7.5 the phenol surface is essentially neutral (pK_a of simple phenols $\sim$10) and could form hydrogen bonds. The influence of hydrogen bonds on protein binding energy through the OH group, most likely, is significantly lower as seen (Figs. 4 and 5) in the example of the aliphatic OH-terminated SAM surfaces. The influence of C═O groups on BSA and IgG adsorption would be de-

pendent on the their orientation on the surface. A preliminary surface-enhanced Raman spectrum (SERS) of the PheOH SAM on the gold surface (spectrum not presented here, will be published later) shows very weak intensity of the C—S and C═O vibrations and relatively strong phenol vibration lines. From surface selection rules it is known that bonds that are oriented parallel to the surface display weaker SERS intensity than those that are oriented perpendicular to the surface. Thus, we conclude that the C—S and the C═O bonds are, on average, oriented parallel to the surface. This suggests that (i) the tilting angle of this aryl-alkyl thiol is much larger than 30° and (ii) the surface of this SAM is defined by the phenol ring and much less by the carbonyl group. We believe that the protein-surface interaction in this case is due to the high value of the interfacial-free energy (1) of the PheOH SAM surface due to π electrons system of the phenolic group. Therefore, this surface adsorption may be facilitated by π electron interactions of the phenolic terminal group of the SAM with π electrons (amide bonds, aromatic amino acids, etc.) on the protein molecules. BSA was adsorbed to a greater extent on this surface than on the CH_3 SAM. One possible reason for this could be the distribution π electron containing residues on BSA's surface. To confirm this supposition additional experiments are in progress.

The COO^- SAM is hydrophilic (the water contact angle is less than 10° (27)). This surface is negatively charged under our experiment conditions. As a rule, hydrophilic surfaces more weakly adsorb proteins (1–3) as compared with hydrophobic surfaces. However, our results show that both hIgG and BSA are significantly adsorbed to this surface as evidenced by surface concentrations only slightly less than that observed for the CH_3 SAM (Figs. 4 and 5, compare curves COO^- and CH_3). This is surprising in light of the fact that at pH 7.4 BSA is net negatively charged ~ -18 (28) and hIgG is slightly positively charged (29). In our experimental conditions (50 m*M* phosphate buffer) not all charges on the proteins are screened by the ions. It is known (1) that electrostatic interactions provide relatively insignificant contributions to protein adsorption at ionic strength >100 m*M* due to the screening of protein charge by counterions. Also noteworthy is the fact that rates of desorption of hIgG and BSA are largest for the COO^- SAM. Since we observe much lower surface concentrations of hIgG and BSA on hydrophilic OH surfaces (Figs. 4 and 5, curves OH), we believe these results suggest that protein-surface interaction is electrostatic. While an electrostatic interaction between the positively charged hIgG and the COO^- SAM is readily rationalized, the case for BSA is not (BSA molecule has three domains with net charges -10, -8 and 0, respectively (28)). It may be, however, that although BSA has a net negative charge, positive charges may still reside on the protein surface and that adsorption could take place at these small positively charged domains. If this is the case, we would expect BSA to be highly oriented on this surface. Finally, desorption rates are consistent with these arguments. Adsorption via small positively charged domains would mean fewer points of attachments, localization of charge, and minimization of denaturation, thus increasing the probability of desorption. In this way the unfolding or denaturation levels of these proteins may be less than on the hydrophobic surface.

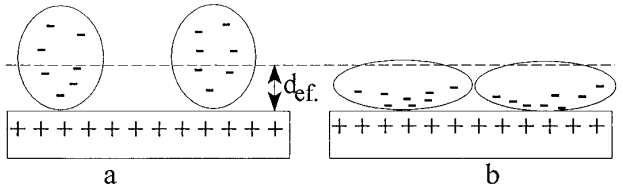

FIG. 8. Cartoon shows possible variant of protein spreading on the surface. Before (a) and after (b) spreading the effective thickness $d_{\text{eff.}}$ of the protein layer can be the same.

The positively charged NH_2 SAM surfaces are as hydrophilic as the COO^- surface (contact angle less than 10°); however significantly less hIaG adsorbed to it (Fig. 4a). A desorption of hIgG is observed on both these surfaces after initiation of washing. For BSA (Fig. 5a), the quantity of protein on NH_2 and COO^- surfaces is approximately the same, and no changes in SPR response upon washing is observed. Moreover, during washing, the kinetic curve increases slightly. (The same effect also was observed for BSA on the PheOH surface.) Possibly it is the process of conformational changes which is being observed after washing was began. As the effective thickness of protein layer cannot increase during the washing, these changes may be due to increasing in the protein layer effective refractive index that can be the result of the proteins spreading (Fig. 8) on the surface. In cases where proteins significantly change conformation during adsorption, Eq. [1] probably cannot be used to calculate surface concentration.

The hydrophilic OH SAM surface (contact angle $\sim 0°$), as was expected, adsorbed significantly lower amounts of the proteins. Under physiological conditions (pH 7.4) the OH group ($pK_a = 13$) of this alkyl thiol retains the hydrogen on the OH group and is able to form hydrogen bonds with side-end groups of polar protein amino acids. Probably a combination of multipoint hydrogen bond formation and the lateral electrostatic repulsion (especially for BSA molecule) are responsible for hIgG and BSA adsorption on the OH surface under our experimental conditions. The low molecular weight ion screening must also be taken into consideration.

The OEO SAM is moderately hydrophilic based on contact angle measurements (25° (32) and our data). The adsorption curves, or more correctly for this case, the SPR shift versus incubation time in protein solutions, for hIgG and BSA on the OEO surface are shown in Figs. 4 and 5 (OEO curves), respectively, and Fig. 6. These data show that ad-

sorption of hIgG and BSA, over a tenfold concentration range (0.5–5 μM), is extremely low. The small SPR shifts observed are due to bulk refractive index changes of the higher protein concentration solutions. (As already mentioned [Fig. 3], the SPR minimum position depends on the bulk refractive index of the medium above the sample surface.) To confirm this, different concentrations of hIgG and BSA were applied (Fig. 6). Using the calibration results (Fig. 3) for water-glycerol solutions and known protein concentrations, the refractive index increment *dn*/*dc* of bulk solution containing protein was estimated. The value determined for *dn*/*dc* was 0.201 mL/mg, which is in very good agreement with the literature (12) (0.182–0.190 mL/mg). From *ex situ* (24, 25) measurements it was not clear how much protein adsorbed reversibly on the OEO surface because the resulting thickness was measured after washing (25) which was capable of removing all reversibly adsorbed proteins. Usually, for a reversible adsorption process and small surface concentrations, kinetic curves do not show fast changes (Fig. 6) at the initial stages of protein adsorption and desorption (when washing was begun). This fact, coupled with the result for value of *dn*/*dc* and no observed changes in SPR width (Fig. 7, curve OEO), suggests that no protein adsorption occurs on OEO SAM surface and supports the idea that this surface is resistant (32) to protein adsorption. Possible mechanisms for the resistance to protein adsorption are based on the interaction of water with the EO chains of the poly-EO (PEO, also referred to as polyethylene glycol [PEG]) and are discussed in (32–34). It was suggested that resistance depends on the polymer molecular weight, surface density, and conformation of the molecule (the dipole-osmotic model (32)). For a well-packed OEO SAM layer, it was also shown (35), that molecular weight is not so important and the resistance does not depend strongly on the number of EO segments of the OEO alkyl thiol. More importantly, however, is the surface density of these segments.

SUMMARY

The nonspecific binding of human immunoglobulin G (hIgG) and bovine serum albumin (BSA) was studied on gold surfaces modified by self-assembled alkyl thiol monolayers (SAMs) with the following terminal groups: CH_3, C_6H_4OH, COO^-, NH_2, OH, and oligoethylene oxide (OEO). The kinetics of hIgG and BSA adsorption and desorption were monitored utilizing the SPR technique with a flow cell. The surface concentration of hIgG molecules adsorbed on the SAMs examined decreased in the order: $CH_3 > C_6H_5OH > COO^- > NH_2 > OH >$ OEO SAM surfaces. Binding of BSA observed to the SAM's surface, decreased in the order: $C_6H_5OH > CH_3 > COO^- > NH_2 > OH >$ OEO. The results suggested that on the OEO SAM, the surface concentration of these proteins was less than 0.5 ng/cm^2 (the detection limit of our SPR device) and approximately 10^3 times smaller than on the hydrophobic CH_3-terminated SAM surfaces.

An increase in the SPR width was observed for surfaces that adsorb proteins. We believed that this is the result of radiative damping of surface plasmons due to increasing molecular level roughness of the sample surface as protein adsorption progresses.

Well-characterized surfaces fabricated using self-assembled monolayers and the SPR technique accompanied with a flow cell gave rise to the possibility of carrying out experiments under standard, reproducible conditions, and in a real-time regime. The resistivity of the OEO SAM surface to protein adsorption may be used in future experiments to create surfaces with specific properties and quantity of active sites that can help in modeling and understanding of protein adsorption on the interfaces.

ACKNOWLEDGMENTS

We thank Dr. A. Gaigalas for help in construction of the SPR device, Dr. R. Ashton and Dr. A. Plant for the discussions during the preparation of this manuscript. This project was supported by a grant (70NANB5H0024) from NIST and Consortium of Advanced Biosensors, a group of Biosensors Manufacturers working with NIST to improve biosensors capabilities.

REFERENCES

1. Andrade, J. D., and Hlady, V., *Advances in Polymer Sci.* **79,** 3 (1986).
2. Norde, W., *Advances in Colloid and Interface Sci.* **25,** 267 (1986).
3. Horbertt, T. A., and Brash, J. L., *in* ''Proteins at Interfaces. Physicochemical and Biochemical Studies'' (J. L. Brash and T. A. Horbett, Eds.), p. 1. American Chemical Society, Washington, D.C., 1987.
4. Sadana, A., and Beelaram, A. M., *Biosensors & Bioelectronics* **10,** 301 (1995).
5. Khilko, S. N., Corr, M., Boyd, L. F., Lees, A., Inman, J. K., and Margulies, D. H., *J. Biological Chemistry* **268,** 15425 (1993).
6. Park, K. D., and Kim, S. W., *in* ''Poly(Ethylene Glycol) Chemistry. Biotechnical and Biomedical Applications'' (J. M. Harris, Ed.), p. 283. Plenum Press, New York, London, 1992.
7. Horsley, D., Herron, J., Hlady, V., and Andrade, J. D., *in* ''Proteins at Interfaces. Physicochemical and Biochemical Studies'' (J. L. Brash and T. A. Horbett, Eds.), p. 291. American Chemical Society, Washington, D.C., 1987.
8. Mueller, H. J., *in* ''Proteins at Interfaces. Physicochemical and Biochemical Studies'' (J. L. Brash and T. A. Horbett, eds.), p. 435. American Chemical Society, Washington, D.C., 1987.
9. Pockrand, I., Swalen, J. D., Gordinii, J. G., and Philpott, M. R., *Surface Sci.* **74,** 237 (1977).
10. Daniels, P. B., Daecon, J. K., Eddowes, M. J., and Pedley, D. G., *Sensors and Actuators* **15,** 11 (1988).
11. Jonson, U., Malmquvist, M., and Ronnberg, I., *J. Colloid Interface Sci.* **103,** 360 (1985).
12. Corsel, J. W., Willems, G. M., Kop, J. M. M., Cuypers, P. A., and Hermens, W. Th., *J. Colloid Interface Sci.* **111,** 544 (1986).
13. Cuypers, P. A., Willems, G. M., Kop, J. M. M., Corsel, J. W., Janssen, M. P., and Hermens, W. Th., *in* ''Proteins at Interfaces. Physicochemical and Biochemical Studies'' (J. L. Brash and T. A. Horbett, eds.), p. 208. American Chemical Society, Washington, D.C., 1987.
14. Martensson, J., and Arwin, H., *Langmuir* **11,** 963 (1995).
15. Malmsten, M., *J. Colloid Interface Sci.* **166,** 333 (1994).

16. Malmsten, M., and Siegel, G., *J. Colloid Interface Sci.* **170,** 1120 (1994).
17. Malmsten, M., *J. Colloid Interface Sci.* **172,** 106 (1995).
18. Hlady, V., and Andrade, J. D., *Colloids and Surfaces* **32,** 359 (1988).
19. Nimeri, G., Lassen, B., Golander, C. G., Nilsson, U., and Elwing, H., *J. Biomater. Sci. Polymer Edn.,* **6,** 573 (1994).
20. Sjolander, S., and Urbaniczky, C., *Anal. Chem.* **63,** 2338 (1991).
21. Glaser, R. W., *Anal. Biochemistry* **213,** 152 (1993).
22. Haynes, C. A., and Norde, W., *J. Colloid Interface Sci.* **169,** 313 (1995).
23. Whitesides, G. M., and Laibinis, P. E., *Langmuir* **6,** 87 (1990).
24. Prime, K. L., and Whitesides, G. M., *Science* **252,** 11641 (1991).
25. Prime, K. L., and Whitesides, G. M., *J. Am. Chem. Soc.* **115,** 10714 (1993).
26. Silin, V. I., Balcytis, G. A., Zhizhin, G. N., and Yakovlev, V. A., *Vibrational Spectroscopy* **5,** 133 (1993).
27. Bain, C. B., Troughton, E. B., Tao, Y.-T., Eval, J., Whitesides, G. M., and Nuzzo, R. G., *J. Am. Chem. Soc.* **111,** 321 (1989).
28. Anfinsen, C. B., Edsall, J. T., and Richards, F. M., ''Advances in Protein Chemistry,'' Vol. 35. Academic Press, Orlando, San Diego, New York, London, 1985.
29. Nezlin, R. S., ''Biochemistry of Antibodies.'' Plenum Press, New York, London, 1970.
30. Tilton, R. D., Robertson, C. R., and Gast, A. P., *J. Colloid Interface Sci.* **137,** 192 (1990).
31. Tilton, R. D., Gast, A. P., and Robertson, C. R., *Biophys. J.* **58,** 1321 (1990).
32. Golander, C.-G., Herron, J. N., Lim, K., Claesson, P., Stenius, P., and Andrade, J. D., *in* ''Poly(Ethylene Glycol) Chemistry: Biotechnical and Biomedical Applications'' (J. M. Harris, Ed.), p. 221. Plenum Press, New York, London, 1992.
33. Jeon, S. I., Lee, J. H., Andrade, J. D., and De Gennes, P. G., *J. Colloid Interface Sci.* **142,** 149 (1991).
34. Jeon, S. I., Lee, J. H., and Andrade, J. D., *J. Colloid Interface Sci.* **142,** 159 (1991).
35. Pale-Grosdemange, C., Simon, E. S., Prime, K. L., and Whitesides, G. M., *J. Am. Chem. Soc.* **113,** 12 (1991).